Transportation Research Part C 94 (2018) 172–184

Contents lists available at ScienceDirect

Transportation Research Part C

journal homepage: www.elsevier.com/locate/trc

Macroscopic Fundamental Diagram for pedestrian networks: Theory and applications

S.P. Hoogendoorn [a,*], W. Daamen [a], V.L. Knoop [a], J. Steenbakkers [b], M. Sarvi [c]

[a] Delft University of Technology, Stevinweg 1, 2628 CN Delft, The Netherlands
[b] INCONTROL Simulation Solutions, Papendorpseweg 77, 3528 BJ Utrecht, The Netherlands
[c] The University of Melbourne, Building 175, Block B, Room 205, Victoria 3010, Australia

ARTICLE INFO

Article history:
Received 12 August 2017
Received in revised form 5 September 2017
Accepted 6 September 2017
Available online 18 September 2017

Keywords:
Macroscopic Fundamental Diagram
Pedestrian networks
Spatial variation of density

ABSTRACT

The Network or Macroscopic Fundamental diagram (MFD) has been a topic receiving a lot of attention in the past decade. Both from a theoretical angle and from a more application-oriented perspective, the MFD has proven to be a powerful concept in understanding and managing vehicular network dynamics.

In particular, the application in traffic management has inspired the research presented in this contribution, where we explore the existence and the characteristics of the pedestrian Macroscopic Fundamental Diagram (p-MFD). This is first of all done from a theoretical perspective, which results in the main contribution of this research showing how we can derive the p-MFD from assumed local fundamental diagrams (FDs). In doing so, we show that we can relate the average (out-)flow from a pedestrian network as a function of the average spatial density $\bar{\rho}$ and the density spatial variation σ^2. We show that the latter is essential to provide a reasonable description of the overall network conditions. For simple relations between density and speed (i.e. Greenshields and Underwood fundamental diagrams), we derive analytical results; for more commonly used FDs in pedestrian flow theory, such as the triangular FD of Newell or the FD of Weidmann, we show the resulting relation by proposing a straightforward simulation approach.

As a secondary contribution of the paper, we show how the p-MFD can be constructed from pedestrian trajectory data stemming from either microsimulation or from experimental studies. We argue that the results found are in line with the theoretical results, providing further evidence for the validity of the p-MFD concept. We furthermore discuss concepts of hysteresis, also observed in vehicular network dynamics, due to the differences in the queue build up and recuperation phases.

We finally present some applications of the presented concepts in crowd management, network level-of-service determination, and coarse-scale modelling.

1. Introduction

The Network or Macroscopic Fundamental Diagram (MFD) for vehicular networks has received a lot of attention in the past decade, gradually leading to a comprehensive theory of network dynamics (Daganzo, 2007; Daganzo and Geroliminis, 2008). Hoogendoorn et al. (2011) has shown that a similar relation exists between the number of pedestrians

* Corresponding author.
E-mail address: s.p.hoogendoorn@tudelft.nl (S.P. Hoogendoorn).

http://dx.doi.org/10.1016/j.trc.2017.09.003
0968-090X/

in an area and the average flow in that area (production). Saberi and Mahmassani (2014) builds upon Hoogendoorn et al. (2010) and also shows that pedestrian crowds have an area-wide fundamental diagram that is similar to a network fundamental diagram of vehicular traffic, using empirical data from experiments. Moreover, they show that in a multidirectional area pedestrian traffic exhibits hysteresis behaviour similar to that of some other many-particle physical systems. The observed hysteresis formed a clockwise loop in which the areawide pedestrian flow was higher during the loading period than during the unloading period.

Pedestrian dynamics are known for its sensitivity to homogeneity of the pedestrian flow composition. Campanella et al. (2009) and Yang et al. (2014) show the consequences of heterogeneity on e.g. breakdown probability (capacity). Similar effects of the spatial variability of vehicle density on urban capacity are found by a.o. Mazloumian et al. (2010) and Daganzo et al. (2011). Homogeneity also plays an important role in the MFD, as the condition that the congestion is spread homogeneously over the network is one of the assumptions under which a proper shape of the MFD is found. Knoop et al. (2015) shows the effect of inhomogeneity by deriving the so-called generalised macroscopic fundamental diagram (GMFD). This effect of inhomogeneity is also found for MFDs for pedestrian traffic. Daamen et al. (2015) considers the effects of spatial inhomogeneity of the density and found that at the same density, a larger spatial variation in density leads to reduced network flows.

However, a thorough theoretical underpinning of the MFD and a quantification of the effect of the spatial distribution of density does not exist yet. This contribution builds upon the before-mentioned exploration of the pedestrian macroscopic fundamental diagram by Hoogendoorn et al. (2011). We explore the concept of the MFD for region-wide pedestrian flow operations (referred to as the p-MFD in the ensuing) and derive a relation between flow, (average network) density and spatial distribution of density. Next to performing several theoretical analyses, we investigate the characteristics of the p-MFD using both experimental and simulation data.

This contribution starts with an overview of the main definitions, followed by theoretical considerations on the p-MFD. Then, the properties of the p-MFD are investigated using data from micro-simulation (Section 4) and data from laboratory experiments (Section 5). We end with an overview of applications of the MFD for pedestrian networks, and conclusions and recommendations.

2. Definitions and nomenclature

Pedestrian flows are two (and in some cases even three) dimensional. This implies that common concepts from – generally one-dimensional – vehicular traffic flow theory, such as flows, speeds, and densities, need to be re-considered carefully before they can be used in a pedestrian flow context. From a macroscopic (or rather, continuum) perspective, concepts such as density, flow and average speed are relatively straightforward to interpret. For an introduction into the key variables for continuum multi-directional pedestrian flow modelling, we refer to Hoogendoorn et al. (2015).

For microscopic analyses using either simulation data or experimental data, concepts are somewhat more ambiguous. Duives et al. (2015) compares nine different definitions of density and shows that the results differ considerably when using the same underlying data set. Johansson (2009) and Zhang et al. (2011) show that these measures to compute the density might introduce dissimilarities between the resulting fundamental diagrams.

In this contribution, we use the concept of Voronoi diagrams (Zhang and Seyfried, 2013) to the microscopic data from either simulations or from experiments to determine the local density and the spatial density variation. Fig. 1 shows an example of the Voronoi diagram. In a Voronoi diagram, each cell corresponds to a single pedestrian p and includes all points in the area closer to pedestrian p than to any other pedestrian. The crosses indicate the locations of the individual pedestrians i at a time instant t_k. The cells are the local regions that reflect the area Ω_i that is available to the pedestrian. For the concepts discussed in this paper, we will modify the standard Voronoi approach in such a way that $\cup_{i=1}^{n}\Omega_i = \mathcal{A}$, where $\mathcal{A}$ is the (two-dimensional) walking area. Having computed the Voronoi diagram, we can define a pedestrian specific density $\rho_i(t_k)$:

$$\rho_i(t_k) = \frac{1}{|\Omega_i(t_k)|}. \tag{1}$$

The average density $\bar{\rho}(t_k)$ for time instant t_k is then given by averaging the pedestrian specific densities $\rho_i(t_k)$:

$$\bar{\rho}(t_k) = \frac{1}{n}\sum_{i=1}^{n}\rho_i(t_k), \tag{2}$$

where n is the amount of pedestrians in the area. As a measure of the spatial density variation $\bar{\sigma}(t_k)$, we use the standard deviation of the local densities, i.e.:

$$\bar{\sigma}(t_k)^2 = \frac{1}{n}\sum_{i=1}^{n}(\rho_i(t_k) - \bar{\rho}(t_k))^2 \tag{3}$$

The region-wide instantaneous mean speed is determined by taking the average speed of all pedestrians present in the region at time instant t_k. For a more thorough discussion on the impact of this definition, as well as alternative definitions, we refer to Duives et al. (2015).

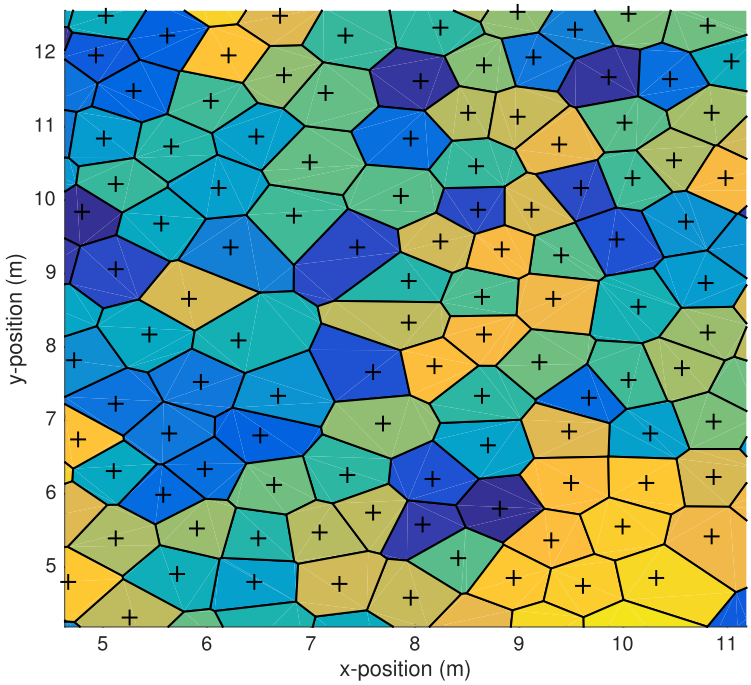

Fig. 1. Example of the Voronoi diagram.

3. Theoretical considerations

The focus of this contribution is the analysis of a network or area wide function describing the overall network operations in terms of flow as a function of some area wide quantities, such as average density. Before investigating if such a relation exists using simulation and experimental data, let us first consider area-wide pedestrian flow operations from a more theoretical perspective.

3.1. Upper bound for MFD for concave FDs

Consider a region $\mathcal{A}$ that is divided into disjoint subregions $\mathcal{A}_i$. Let us assume that for each of these subregions, pedestrian flow operations can be adequately described by a fundamental relation $q = Q(\rho)$, where q denotes the average flow (in P/s) and ρ denotes the density (in P/m^2). We assume that this function is concave. For the sake of simplicity, we will for now not consider multi-directional flows. With knowledge of the density ρ_i in a subregion $\mathcal{A}_i$, we can thus determine the flow by applying the fundamental diagram.

Let us now consider the complete region $\mathcal{A}$. Assuming that all m subregions have the same area, we get:

$$\bar{\rho} = \frac{1}{m}\sum_{i=1}^{m}\rho_i. \tag{4}$$

Since $Q(\rho)$ is concave, we have according to Jensen's inequality:

$$\bar{q} = \frac{1}{m}\sum_{i=1}^{m}Q(\rho_i) \geqslant Q(\bar{\rho}). \tag{5}$$

This means that the local fundamental diagrams will form the upper bound of an eventual relation between the region-average density $\bar{\rho}$ and a region-average flow $\bar{q}$.

3.2. Analytical derivation of the pedestrian macroscopic fundamental diagram

More precise approximations can be made assuming specific local fundamental relations. For the sake of argument, let us assume that the following local fundamental diagram (suggested by Greenshields (1947)) applies for the subregions $\mathcal{A}_i$:

$$Q(\rho) = v^0 \rho \left(1 - \frac{\rho}{\rho_{jam}}\right). \tag{6}$$

If we want to determine a relation between $\bar{q}$ and $\bar{\rho}$, again assuming that all subregions have the same area, we get:

$$\bar{q} = \frac{1}{m}\sum_{i=1}^{m} Q(\rho_i) = \frac{1}{m}\sum_{i=1}^{m} v^0 \rho_i \left(1 - \frac{\rho_i}{\rho_{jam}}\right). \tag{7}$$

Some straightforward calculations reveal that:

$$\bar{q} = v^0 \bar{\rho}\left(1 - \frac{\bar{\rho}}{\rho_{jam}}\right) - \frac{v^0}{\rho_{jam}}\sigma^2 = Q(\bar{\rho}) - \frac{v^0}{\rho_{jam}}\sigma^2, \tag{8}$$

where

$$\sigma^2 = \frac{1}{m}\sum_{i=1}^{m}(\rho_i - \bar{\rho})^2. \tag{9}$$

is the spatial density variation. Eq. (8) shows the existence of a function $\bar{q} = \tilde{Q}(\bar{\rho}, \sigma^2)$ that relates the region wide flow to the region wide density and spatial density variation. We can see that the spatial variation has a negative impact on the (maximum) network production. The implies that the network capacity is conditional on the spatial variation as well.

As a direct consequence, a function relating the region wide flow to the region wide density will only exist if the spatial density variation is a function of the region wide density, i.e. $\sigma = \Sigma(\bar{\rho})$. This will hold if the spatial distributions of the pedestrian flows over the areas are the same for a specific network load (average density) in each case, and for each moment in time (including when the network is loaded and unloaded), see also Geroliminis and Sun (2011). In many cases, this will *not* be the case due to differences in bottleneck activation during loading and unloading of the network, temporal differences in demand patterns for different times of the day, etc. Hence, often, the spatial density variation would have to be explicitly considered in the representation of the region wide relation between region wide flow parameters. Note that in Section 6.3, we briefly revisit this issue. Also note that this whole reasoning holds for vehicular traffic as well.

3.3. Analytical derivation for generic local fundamental diagrams

The Greenshields fundamental diagram has the nice property that it allows derivation of a p-MFD that only depends on the average density and the spatial density variation; it is independent on the specific spatial density distribution. In this section, we illustrate how the result can be generalised to other fundamental diagrams if we assume a specific distribution of the density across the considered area.

Let us again consider a region $\mathcal{A}$ divided into equally small subareas $\mathcal{A}_i$. We assume that the subareas are small enough to allow assuming that the distribution of the density in the subarea is homogeneous. Let $f(\rho) = f(\rho; \bar{\rho}, \sigma^2)$ denote the (empirical) probability density function of the distribution that stems from the densities ρ_i at the subareas. Using this representation, the mean density and spatial density variation can be determined by:

$$\bar{\rho} = E(\rho) = \int \rho f(\rho) d\rho \tag{10}$$

and:

$$\sigma^2 = E((\rho - \bar{\rho})^2) = \int (\rho - \bar{\rho})^2 f(\rho) d\rho \tag{11}$$

respectively.

For the p-MFD, we then have:

$$\bar{q} = E(Q(\rho)) = \int Q(\rho) f(\rho) d\rho. \tag{12}$$

The expression shows the dependence of the shape of the spatial distribution of the density as reflected by $f(\rho)$. Revisiting the p-MFD based on the Greenshields fundamental diagram (Eq. (6)), we note that:

$$\bar{q} = \tilde{Q}(\bar{\rho}, \sigma^2) = \int v^0 \rho \left(1 - \rho/\rho_{jam}\right) f(\rho) d\rho. \tag{13}$$

For the Greenshields local FD, we can now easily show that:

$$\bar{q} = v^0 E(\rho) - \frac{v^0}{\rho_{jam}} E(\rho^2) = v^0 \bar{\rho}\left(1 - \bar{\rho}/\rho_{jam}\right) - \frac{v^0}{\rho_{jam}}\sigma^2, \tag{14}$$

which is equal to the previously derived expression (8).

For other specifications of the fundamental diagram, it will not always be possible to derive an analytical expression. For some specific combinations of local fundamental diagrams $Q(\rho)$ and distribution functions $f(\rho)$, we may however be able to derive the MFD analytically. Let us consider the following example.

We assume that the densities are uniformly distributed on the interval $[\bar{\rho} - \sigma\sqrt{3}, \bar{\rho} + \sigma\sqrt{3}]$. If we, for instance, use the fundamental diagram of Underwood (1961):

$$Q(\rho) = \rho U(\rho) = \rho \cdot e^{b_0 + b_1 \rho}, \tag{15}$$

where $b_0 = \ln(v^0)$ and $b_1 < 0$ are the parameters of the model. We can, after an involved but straightforward calculation, derive:

$$\bar{q} = \frac{\sinh(b_1\sigma\sqrt{3})}{b_1\sigma\sqrt{3}} Q(\bar{\rho}) + \left(\cosh(b_1\sigma\sqrt{3}) - \frac{\sinh(b_1\sigma\sqrt{3})}{b_1\sigma\sqrt{3}}\right)\frac{U(\bar{\rho})}{b_1} \tag{16}$$

Eq. (16) shows that for this specific case and under these specific assumptions, we can derive the p-MFD as a function of the mean density $\bar{\rho}$ and the spatial density variation σ^2. For relatively small values of σ^2 we can use a Taylor series approximation and compute:

$$\bar{q} = Q(\bar{\rho}) + b_1\left(\frac{5}{2}U(\bar{\rho}) + \frac{1}{2}b_1 Q(\bar{\rho})\right)\sigma^2. \tag{17}$$

Since $b_1 < 0$, we see that $\bar{q} < Q(\bar{r})$ due to the impact of the spatial variation as long as $5U(\bar{\rho}) > b_1 Q(\bar{\rho})$. This will be the case for the part of the Underwood fundamental diagram which is convex (i.e. for small enough values of ρ).

It is left to the reader to show that using the Greenshields fundamental diagram will again result in Eq. (8) upon assuming a uniform distribution; the derivation for a bi-linear fundamental diagram is given by Knoop et al. (2015); note that in this case, the impact of the spatial variation is not described explicitly.

3.4. Simulation approach for generic fundamental diagrams

The approaches presented in the previous sections can only be applied to specific functional forms of the local fundamental diagram. For other specifications, an analytical expression can generally not be determined and we have to resort to other approaches such as simulation. Nonetheless, we can easily determine how spatial variation in the density changes the network flow using a simple sampling approach described below.

For the sake of illustration, we will assume a bi-linear local fundamental diagram, specified by:

$$Q(\rho) = \begin{cases} v^0 \cdot \rho & \rho < \rho_{crit} \\ \beta \cdot \left(1 - \frac{\rho}{\rho_{jam}}\right) & \rho \geqslant \rho_{crit} \end{cases} \tag{18}$$

with:

$$\beta = v^0 \cdot \frac{\rho_{crit} \cdot \rho_{jam}}{\rho_{jam} - \rho_{crit}}. \tag{19}$$

Here, v^0 is the free speed, ρ_{crit} is the critical density (density at capacity), and ρ_{jam} is the jam density.

The simulation approach entails drawing the densities ρ_i for region $\mathcal{A}_i$ from some distribution function $F(\rho) = F(\rho; \bar{\rho}, \sigma^2)$ that is characterised by a mean density and variation value. E.g., we could assume that the densities are uniformly distributed around the mean density value. We have applied this procedure to the bi-linear fundamental diagram to analyse the influence of spatial variation in the density. Fig. 2 shows the result of this analysis, using a local fundamental diagram with $u_0 = 1.5$ m/s, $\rho_{crit} = 1.25$ P/m^2 and $k_{jam} = 5.4$ P/m^2.

The impact of the spatial density variation σ^2 is clear, and causes a reduction of the network flow, in particular around the critical density. Note that for higher densities, the linear form of the FD causes σ^2 not to have an impact. This applies equally for low densities, as long as all densities ρ_i are smaller than the critical density. This supports our earlier finding that the relation between the region-average density and a region-average flow will be bounded by the local fundamental diagrams.

Note that similar results are obtained using more common local fundamental diagrams for pedestrian flow. In illustration, Fig. 3 shows the resulting p-MFD when we use the fundamental diagram of Weidmann (1993):

$$U(\rho) = v^0 \cdot \left[1 - \exp\left(-1.913 \cdot \left(\frac{1}{\rho} - \frac{1}{\rho_{jam}}\right)\right)\right]. \tag{20}$$

Also for this local fundamental diagram, we clearly see the impact of the spatial variation in the density.

Note that both examples show how the network maximum production (capacity) will depend on the spatial density variation. Note that the average network density under which the capacity is achieved (the network critical density) also

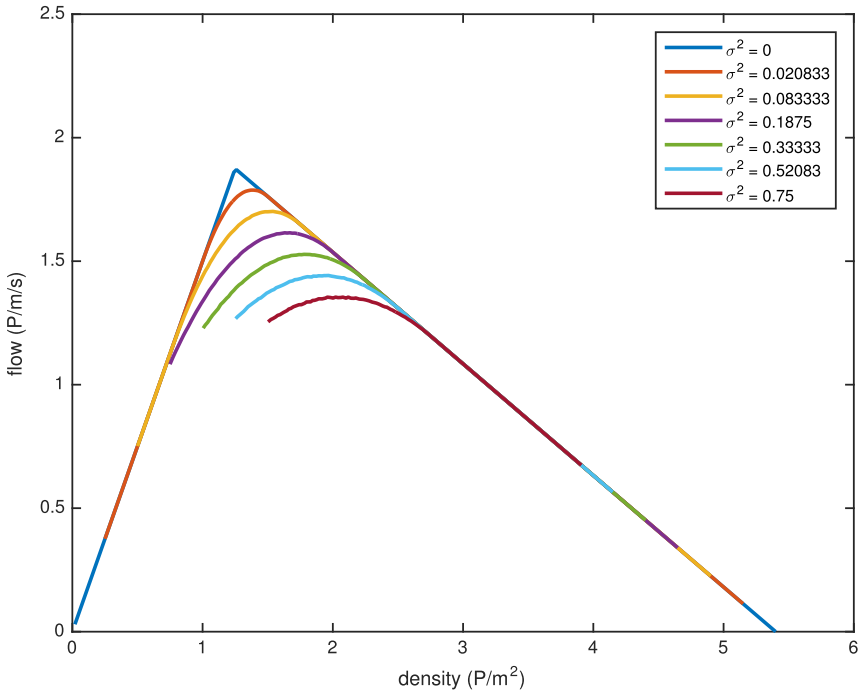

Fig. 2. Impact of spatial density variation on the p-MFD.

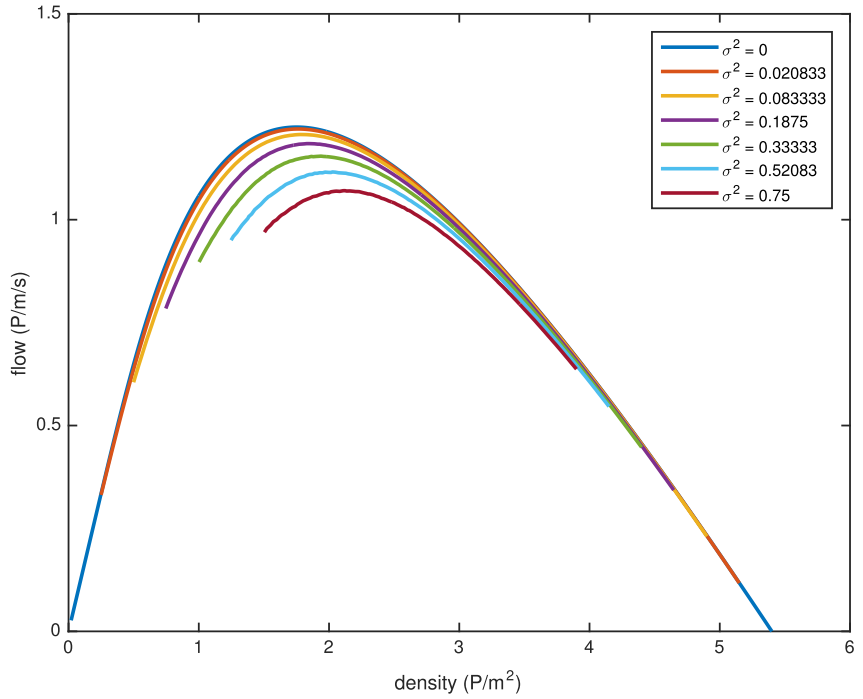

Fig. 3. Impact of spatial density variation on the p-MFD using the local fundamental diagram of Weidmann (1993).

depends on the spatial variation of the density. This has implications for instance control: while decreasing the spatial density variation will increase the capacity, attaining the capacity (e.g. using perimeter control) requires knowledge of σ^2 to be able to steer the state to the network wide sweet spot.

3.5. Reflection

In this section, we have shown how we can derive either analytically or numerically the p-MFD. In doing so, we made assumptions on both the shape of the local FD (to allow analytical derivation of the p-MFD), and in some occasions on the distribution of the densities (e.g. assuming a uniform distribution). For the numerical approach, these assumptions can be relaxed and more generic results can be provided. However, there are still some assumptions left that require further testing. One of these is the fact that we assume that for each location in the network, the local FD is equal. Although this will not be the case in general (e.g. the FD will depend on the composition of the flow), in the remainder we will see if the concept of the p-MFD is meaningful for more realistic cases where these assumptions may not hold.

In the next sections, we will look at p-MFDs derived using data from simulations (Section 4) and from experiments (Section 5). These data analyses should reveal the impact of our findings in more practical settings, in particular showing which levels of spatial variation are to be expected for realistic cases and how these affect average network production.

4. Microscopic simulation analyses

To support the theoretical derivations of the p-MFD in the previous section, this section derives p-MFDs using simulation data. Here, we focus on the relation between the flow and the spatial distribution of the density. We first use the microscopic pedestrian simulation tool NOMAD to simulate relatively simple crossing flows (Section 4.1) and bi-directional flows (Section 4.2), while in Section 4.3 a dataset from a more complex evacuation of an event terrain is applied using PedestrianDynamics.

4.1. p-MFD for crossing flows using NOMAD

The first experiment presented in this contribution conveys results from simulations using the NOMAD model (Hoogendoorn and Bovy, 2002, 2003). This microscopic simulation model, bearing resemblance to the social forces model by Helbing and Molnar (1995), produces pedestrian trajectories $\vec{r}_i(t)$ for each simulated pedestrian. Using these trajectories, we compute the local densities $\rho_i(t_k)$, the average density $\bar{\rho}(t_k)$ for each time instant of interest, and the spatial density standard deviation $\sigma(t_k)$.

The case entails pedestrians coming from four different directions. The flow is gradually increased, in the end leading to flow breakdown. For more details, see Hoogendoorn et al. (2011).

Fig. 4 shows different relations in the data, including the MFD speed-density and flow-density relations $U(\bar{\rho})$ and $Q(\bar{\rho})$ for a *crossing flow* simulation experiment. We can observe that the data suggest the existence of an MFD for pedestrian flow. In

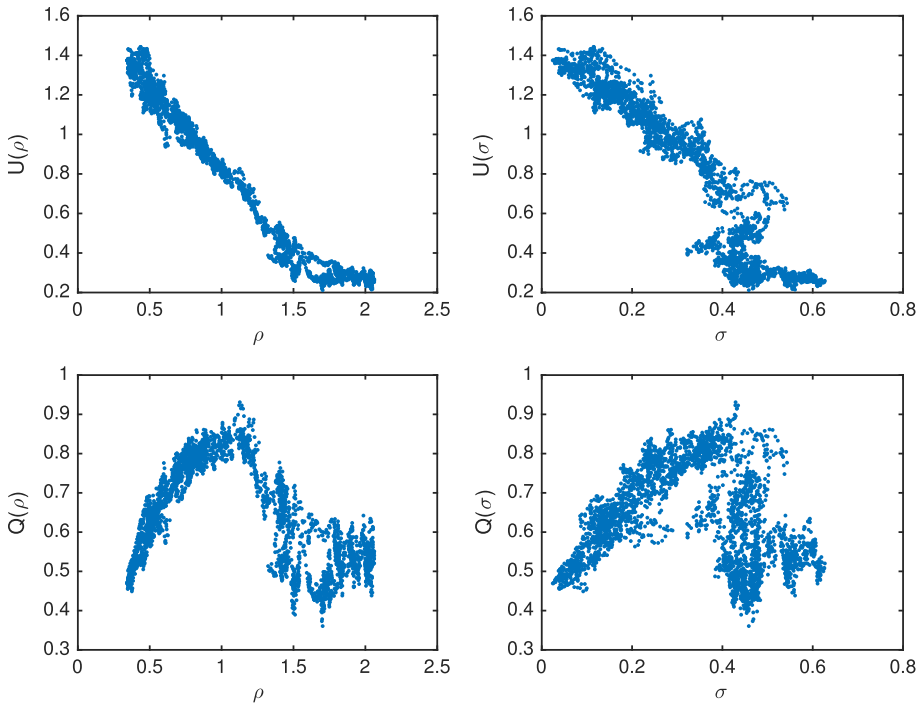

Fig. 4. Fundamental relations for crossing flow experiment.

particular for higher average densities, the relation becomes less crisp and a hysteresis loop occurs, which in particular is clear for the flow-density curve. A similar hysteresis loop was found by Saberi and Mahmassani (2014).

Looking in more detail, Fig. 5 shows the complex dynamics of the area-wide pedestrian operations at higher densities. The $(\bar{\rho},\sigma)$-path shows that in the build up phase (around $t = 245$ s), the spatial variation is relatively low and the flow is relatively high. During the congestion build up phase, both the average density and the spatial variation quickly increase to very high levels. Upon recuperation (from say $t = 300$ s onward), the spatial variation of the density remains higher, while the flow stays lower (compared to the build up phase).

To gain further insight into the form of the MFD for this specific case, we applied multi-variate regression to the high density data, yielding the following relation:

$$\tilde{Q}(\bar{\rho},\sigma) = 0.87 - 0.14 \cdot \bar{\rho} - 0.19 \cdot \sigma^2, \tag{21}$$

with $R^2 = 0.72$ for $1.2\ \mathrm{P/m^2} \leqslant \bar{\rho} \leqslant 5\ \mathrm{P/m^2}$, showing how the spatial variation of the density influences the area-wide flow at high densities. All parameters are significant at a 95% level of significance. For lower densities $\bar{\rho} < 1.2\ \mathrm{P/m^2}$, we have determined the following relation:

$$\tilde{Q}(\bar{\rho},\sigma) = 1.43 \cdot \bar{\rho} - 0.62 \cdot \bar{\rho}^2 - 0.23 \cdot \sigma^2, \tag{22}$$

with $R^2 = 0.93$. Note that for both free flow and congested conditions, the influence of the spatial density variation on the area wide flow (and speed) is (statistically) significant (at 95% level of significance). The cut-off value of $1.2\ \mathrm{P/m^2}$ was determined by looking at the fundamental diagram and judging what a reasonable value for the critical density was.

Note that these results appear to be in line with the theoretical analysis showing that the area-wide flow is negatively correlated with the spatial density variation. Since the free-flow branch of a pedestrian FD can be reasonably well described by a linear relation between density and speed, i.e.:

$$U(\bar{\rho}) = v^0 - \eta \cdot \bar{\rho}, \tag{23}$$

which yields a second-order relation between flow and density, the theoretical result using the Greenshields FD described earlier is likely to provide a reasonable approximation. As a result, the form $\tilde{Q}(\bar{\rho},\sigma^2) = Q(\bar{\rho}) - \gamma \cdot \sigma^2$ can actually be justified to describe the free flow branch of the p-MFD.

For this specific case (i.e., use of NOMAD simulation model, consideration of a crossing-flow scenario, chosen parameter values), the impact could be described as a linear relation with the spatial density variation σ^2, where $\tilde{Q}(\bar{\rho},\sigma^2) \approx Q(\bar{\rho}) - 0.21 \cdot \sigma^2$. If we compare this result to the theoretical result using the Greenshields fundamental diagram,

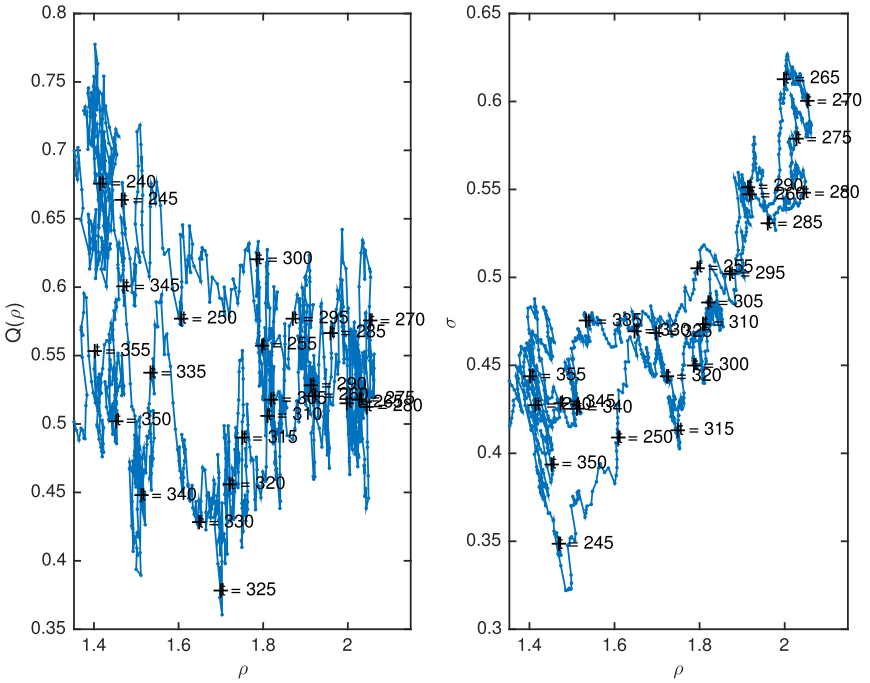

Fig. 5. Flow-density relation at higher densities and (ρ,σ)-path.

where $\tilde{Q}(\bar{\rho},\sigma^2) \approx Q(\bar{\rho}) - v^0/\rho_{jam} \cdot \sigma^2$, we can conclude that this result is plausible and that the impact of the spatial variation σ^2 from the experiment is in line with the theoretical result, since $v^0/\rho_{jam} \approx 1.34/5.4 = 0.248$.

Based on this, as well as the theoretical result presented earlier, we argue that the spatial variation cannot be excluded in an adequate description of the area-wide flow operations.

4.2. Bi-directional flow experiment

Using the same approach, we performed a bi-directional flow experiment using the NOMAD microsimulation model, using the same parameter set as for the crossing flow experiment. In this case, since self-organisation did not break down, no severe congestion occurred, although some evidence of hysteresis occurring at near critical density was found (not shown). A sensible relation between average network flow, spatial density, and spatial density variation could be established:

$$\tilde{Q}(\bar{\rho},\sigma) = 1.42 \cdot \bar{\rho} - 0.64 \cdot \bar{\rho}^2 - 0.15 \cdot \sigma^2 \tag{24}$$

for $\bar{\rho} < 1.2$ P/m^2, with $R^2 = 0.94$. Again, all parameters turned out to be significant at a 95% level of significance. Note the similarity between the p-MFD estimate for the crossing flow (under free flow) and the bi-directional flow: the free speed v^0 was very similar (1.42 m/s for the bi-directional and 1.43 m/s for the crossing flow); the parameter η describing the reduction of the speed as the density increases was also nearly identical (0.64 [1/Pm^3 s] vs. 0.62 [1/Pm^3 s]); the most considerable difference was the impact of the spatial density variation, expressed by the parameter γ, which is equal to 0.15 m^3/Ps for the bi-directional case and 0.23 m^3/Ps for the crossing-flow case. Although the difference is not huge, at this stage we cannot conclude that a single p-MFD relation could be determined from different flow configurations.

4.3. p-MFD for an evacuation using PedestrianDynamics

The previous section showed the influence of the spatial density variation on the p-MFD for relatively simple crossing flow and bi-directional flow situations. Here, we perform similar analyses for the more complex case of the evacuation of an event terrain. Fig. 6 shows the visualisation of the simulation model, with the event terrain configuration and the locations of the pedestrians at the start of the evacuation (left) and during the evacuation (right).

The results show very limited congestion during the simulation. Using multivariate regression analysis, we fitted the following p-MFD relation:

$$\tilde{Q}(\bar{\rho},\sigma^2) = 2.01 \cdot \bar{\rho} - 0.64 \cdot \bar{\rho}^2 - 0.18 \cdot \sigma^2, \tag{25}$$

where $\bar{\rho} < 1.2$ P/m^2, with $R^2 = 0.79$. Again, all parameters are statistically significant.

Again, we can conclude that a sensible relation between flow, spatial density, and spatial density variation can be derived. The free speed value 2.01 m/s reflects the fact that pedestrians are moving faster due to the evacuation conditions; the other parameters are surprisingly close to the values for the simpler microsimulation case studies.

5. Experimental analyses

To see whether the p-MFD can also be derived for real-life situations (i.e., non-synthetic data), this section considers data from walking experiments. We consider a number of different experiments of varying complexity. More specifically, we consider two experiments: the crossing flow experiment from Hoogendoorn and Daamen (2005), and the merging flow experiment described in Haghani and Sarvi (2016).

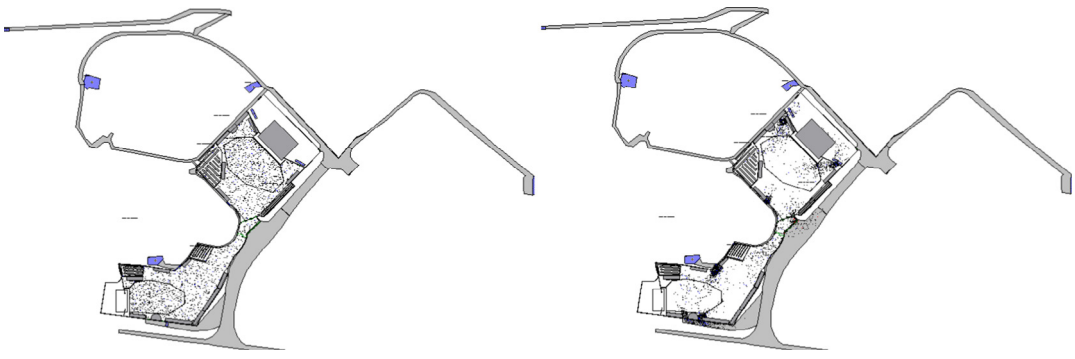

Fig. 6. Visualisation of the evacuation of an event terrain. (a) At the start of the evacuation; (b) during the evacuation.

Experimental research entails interfering with natural processes to obtain more insight into the causal relations between the independent process variables (stimuli) and the observed phenomena (response). By performing experiments we can determine the causes and relations that determine the behaviour of pedestrians. Apart from the methodological advantages, experiments allow observations of conditions that are not available, or are very difficult to observe, in normal conditions. The process variables are both the input and output variables that are deemed relevant.

5.1. Crossing flow experiment

In this case, the important primary factors have been determined from expert knowledge and literature surveys; for details, see Daamen and Hoogendoorn (2003). In the end, pedestrian trajectories are determined from the video imagery. These trajectories are the most elementary and most valuable unit of analysis in traffic flow research and provide all information required for analysis of both the microscopic and macroscopic characteristics.

In total, 10 different walking experiments were performed. In each of these experiments, approximately 60–90 individuals were involved. The participants were divided into eight groups, which were given separate walking tasks for each experiment (walk slowly, walk fast, etc.). The groups themselves were heterogeneous, and consisted of men and women of different ages. The group participants were indicated by the colour of their caps (red or green). The red caps convey the ordinarily behaving pedestrians, while the green caps belonged to pedestrians that had to follow specific instructions (walk aggressively, walk slowly, etc.). The groups were not used to indicate the walking direction, as this could be determined from the video images straightaway. For a detailed description of the experimental setup, see Daamen and Hoogendoorn (2003).

For the sake of illustration and comparison with the microscopic simulation outcomes, we here consider only the crossing flow experiment. Using the same approach as described before, we establish the following relation between region-wide flow, density and spatial density variation:

$$Q(\bar{\rho},\sigma) = 1.63 \cdot \bar{\rho} - 0.41 \cdot \bar{\rho}^2 - 0.28 \cdot \sigma^2, \tag{26}$$

with $R^2 = 0.86$, for $\bar{\rho} < 1.2$ P/m^2. Note that the relation resembles the free flow branch of the diagram based on the simulation experiments presented above. Also note that congestion did not occur in this experiment. Therefore, we only derived a single regression line. Moreover, we could not identify any form of hysteresis.

5.2. Merging flow experiment

To understand pedestrian behaviour negotiating through conflicting geometries a large number of experiments under controlled laboratory conditions were performed in which certain factors such as desired speed level, the angle between two merging branches and merging design are considered. The experiments were performed in 2015 in Melbourne, Australia. In order to make the duration of the experiments long enough to observe stationary state and reproduce high-density conditions, the experiments were performed with up to 150 participants. All experiments were recorded by several cameras which were mounted 9 m above the floor. In merging layouts, two streams meet each other either symmetrically or asymmetrically and form a single stream. The widths of all three corridors were set the same for each of the experimental setups to have uniform streams (1.4 m). The number of participants in the right and left branches was nearly equal. Symmetric configurations include merging setups in which two streams meet each other symmetrically. In the second type of layouts, a straight branch is joined by a deviated branch (i.e. the asymmetric setup). The geometric layouts we examined included symmetric 90°, 180°, 270°, and asymmetric 45° and 90° branches. At the start of the experiments, participants are held in the waiting area and when the experiment begins they were asked to pass a 2 m passage and enter the merging setup. Two different speed regimes were examined, normal walk (as a normal condition with speeds around 1.5 m/s) and run (as a proxy of escape conditions with speeds around 3 m/s). The participants were told the speed regime for each run right before starting each run of the trials. Each run of the experiments was repeated twice and in total, 20 runs of trials were performed. More information on these experiments can be found in Haghani and Sarvi (2016).

In this case, we consider a normal walk situation where two flows merge at 45°. Because of the high demands from both approaches, congestion occurs on either of the incoming approaches. Looking at the speed and flow as a function of both $\bar{\rho}$ and σ, we clearly see the dependence on either of the independent variables. We can also clearly see the hysteresis effect: in the build up of congestion, the flows and speeds are substantially higher than in the recuperation phase. This is in part explained by the fact that the congestion of the two approaches does not resolve at the same pace. As a result, the spatial variation is larger in the recuperation phase than in the build up phase.

We have fitted the p-MFD on the data, and fitted the same polynomial. We find:

$$Q(\bar{\rho},\sigma) = 1.35 \cdot \bar{\rho} - 0.60 \cdot \bar{\rho}^2 - 0.20 \cdot \sigma^2. \tag{27}$$

Again, we can clearly see the impact of the spatial density variation on the p-MFD; although different from the crossing flow experiment, the order of magnitude is similar. Note that although there was some congestion, we had too few data points for $\bar{\rho} > 1.2$ P/m^2 to fit the congested branch of the FD.

In conclusion to this section, we see that the p-MFD concept is also plausible for real data, in this case stemming from different pedestrian experiments. This concludes the analysis supporting the existence of the p-MFD and its characteristics. Using these results, we briefly explore some of the applications of the p-MFD in the final part of this contribution.

6. Applications of the p-MFD

Let us in this section briefly consider some applications of the p-MFD. Specifically, we will consider the network-wide determination of the Level-of-Service, applications to crowd control, modelling the coarse dynamics in pedestrian networks, and judging the performance of pedestrian flow models.

6.1. MFD for Level-of-Service analysis

Determining the Level-of-Service (LOS) for a walking facility is often done using cross-sectional or small area measurements (Daamen and Hoogendoorn, 2006). Using these measurements, the Level-of-Service of that particular cross-section or small area can be determined.

The MFD provides the opportunity to determine a global LOS for a larger area in a meaningful and consistent way. One of the advantages is that local disturbances will only be picked up when the resulting LOS deterioration is considerable. Including the spatial density variation allows for inclusion of those local bottlenecks that have a network-wide impact on the production.

6.2. Crowd control

In the previous sections, we have seen that the shape of the p-MFD can be very different from the one area to the next, based on the function, design, and use of the area. Some areas show a strong reduction in the performance when the accumulation surpasses some critical accumulation, while other areas show a much more constant performance even if the accumulation increases.

For crowd control applications, it is important to keep the overall performance of the area as high as possible. In the Schiphol Plaza situation (the landside hub of Amsterdam Airport Schiphol), for instance, we see that crowding problems occur in a specific area (the court, see Daamen et al., 2008). From a crowd-control perspective, it seems logical to limit the inflow into that area such that the performance stays at a high level. This has an effect on the subarea (the throughput stays high) and on the overall network (the spatial variation in the density is reduced).

The following control law will keep the performance of the area at the maximum level:

$$q_{max}(t) = q_{max}(t-1) - \alpha \cdot \left(n(t) - n'_{crit}\right). \tag{28}$$

Eq. (28) shows that when the accumulation surpasses the critical value n'_{crit}, the maximum inflow q_{max} into the area will be reduced. The maximum inflow will be increased again when the accumulation is less than the critical accumulation.

In this contribution, we have seen that the p-MFD is not only a function of the average density, but also of the spatial variation in the density. This has implications for crowd control, as was already briefly mentioned. In particular, the fact that the network capacity is conditional on the spatial variation, as is the critical density (or accumulation) determines to a considerable extent how for instance perimeter control described earlier should be executed. For the example above, this would mean that we would need to determine $n'_{crit} = n'_{crit}(\sigma^2)$ and determine σ^2 for a particular situation. However, other measures, such as giving information, could also spread a crowd better over the area.

6.3. Coarse dynamics modelling

As a next application example of the p-MFD, we consider dynamic modelling. The basic concept is that we can divide the considered area $\mathcal{A}$ which we want to model into disjoint subareas $\mathcal{A}_j$ with $j = 1, \ldots, m$. For each of these subareas, we can establish p-MFDs.

Suppose that for a specific area $\mathcal{A}_i$, we are only interested in the coarse dynamics. Neglecting the effect of σ^2, in this case, we can use the p-MFD to describe the outflow/ number of completed trips. Let $F_i(n_i(t))$ again denote the outflow of the area as a function of the accumulation $n_i(t)$ in the area. For the accumulation $n_i(t)$ we can then establish the following dynamic equation:

$$\frac{dn_i}{dt} = \sum_j f_{ji}(t) - F_i(n_i(t)), \tag{29}$$

where $f_{ji}(t)$ denotes the outflow from area $\mathcal{A}_j$ to $\mathcal{A}_i$. Now, we let $\phi_{ij}(t)$ denote the share of the outflow from area $\mathcal{A}_i$ to $\mathcal{A}_j$. We can then write:

$$f_{ij}(t) = \phi_{ij}(t) F(n_i(t)). \tag{30}$$

Taking the influence of σ^2 into account is not trivial, and requires more advanced modelling. First of all, we would have $F_i = F_i(n_i(t), \sigma_i^2(t))$ describing the outflow from the area. This is relatively straightforward considering the approaches described in this paper. Second of all, we would need to determine an (approximate) relation describing the dynamic of the spatial variation. In some cases, this may be a static relation, e.g. where the spatial variation is only dependent on the average density in the area. In other cases, more involved relations are to be sought for, e.g. where the spatial variation depends on the average density as well as the temporal change in the average density, e.g.:

$$\sigma^2 = \sigma^2(\bar{\rho}, d\bar{\rho}/dt). \tag{31}$$

The dependence on the derivative $d\bar{\rho}/dt$ reflects the fact that fast changes in the average density due to e.g. high inflows/outflows at the boundaries of the area are likely to lead to large spatial variations in the density. In illustration, for the NOMAD crossing flow experiment, statistical analyses reveal the following relation:

$$\sigma(\bar{\rho}, d\bar{\rho}/dt) = 0.277 \cdot \bar{\rho} - 0.039 \cdot d\bar{\rho}/dt. \tag{32}$$

This relation reveals the nature of the hysteresis loop that we saw before, where in the congestion build up phase ($d\bar{\rho}/dt > 0$) the spatial variation is *smaller* than in the congestion dissipation phase ($d\bar{\rho}/dt < 0$).

6.4. Judging performance of pedestrian flow models

The final application we will illustrate is the application to model calibration and validation. The p-MFD of a specific area $\mathcal{A}$ describes the coarse pedestrian flow behaviour within this area. It summarises the main flow characteristics of the area. When calibrating or validating a pedestrian flow model, the ability of a model to replicate the empirical p-MFD is essential for realistic model outcomes. This holds for pedestrian flow models, but equally for vehicular traffic models.

7. Conclusions and recommendations

In this contribution, we have provided results showing the existence and characteristics of the pedestrian Macroscopic Fundamental Diagram (p-MFD). Our theoretical analyses show that the p-MFD is encapsulated by the local fundamental diagrams (with appropriate scaling). For specific local fundamental diagrams, more precise results could be established showing the relation between the region wide flow, the region wide density and spatial density variation. In particular the spatial density variation turns out to be pivotal in accurately describing the p-MFD. These theoretical analyses form the main contribution of the study. In the future, we could think of including the direction in the spatial variation as well. Moreover, as there is still a fundamental discussion on the fundamental diagrams and their generalisation to different scenarios, further insights into the impact of fundamental diagrams other than the ones presented in this paper on the p-MFD will be elaborated upon.

Furthermore, as a secondary contribution of the study, we show how the p-MFD can be constructed from microscopic pedestrian data stemming from either microsimulation or from experimental studies. We have seen that the results found are in line with the theoretical results, providing convincing evidence for the validity of the p-MFD concept. This holds to the extent that the parameter values found when fitting a relation to the p-MFD data are comparable to those values found in the theoretical analyses. This provides evidence that the theoretical results established using simple local FDs can be used in practical situations as well, although more thorough analyses would be required to make the claim stronger.

An interesting observation was made when comparing the fitted p-MFD functions for different experiments. While it appears that the functions are quite similar – also in terms of the actual parameter values – in particular the impact of the spatial density variation on the average network flow levels needs to be investigated further, as the impact is likely to be dependent on the flow configuration.

We also have identified hysteresis phenomena caused by the differences in queue build up and recuperation phases. Since the number of scenarios considered in which heavy congestion occurred was limited, more investigations are required on this specific topic.

We also presented some applications of the presented concepts in crowd management, network level-of-service determination, and coarse-scale modelling.

Acknowledgements

The research leading to these results has received funding from the European Research Council under the European Union Horizon 2020 Framework Programme for Research and Innovation. It is established by the Scientific Council of the ERC Grant Agreement No. 669792 (ALLEGRO).

References

Campanella, M., Hoogendoorn, S.P., Daamen, W., 2009. Effects of heterogeneity in self-organized pedestrian flows. Transp. Res. Rec.: J. Transp. Res. Board 2124, 148–156.

Daamen, W., Hoogendoorn, S.P., 2003. Experimental research of pedestrian walking behavior. Transp. Res. Rec.: J. Transp. Res. Board 1828, 20–30.

Daamen, W., Hoogendoorn, S.P., 2006. Transfer crowdedness in Dutch train stations: identifying comfort and capacity bottlenecks. In: van Zuylen, H.J. (Ed.), Conference Proceedings 9th TRAIL Congress, TRAIL in Motion. TRAIL Research School, Delft, pp. 1–15.
Daamen, W., Hoogendoorn, S.P., Campanella, M.C., 2008. Assessing pedestrian flow conditions in Schiphol Plaza: can Schiphol Plaza cope with future traveller demands? In: van Zuylen, H.J., van Binsbergen, A.J. (Eds.), Proceedings 10th TRAIL-Congress, TRAIL in Perspective. TRAIL Research School, Delft, pp. 1–15.
Daamen, W., Knoop, V.L., Hoogendoorn, S.P., 2015. Generalized macroscopic fundamental diagram for pedestrian flows. In: Chraibi, M., Boltes, M., Schadschneider, A., Seyfried, A. (Eds.), Traffic and Granular Flow '13. Springer International Publishing, Switzerland, pp. 41–47.
Daganzo, C.F., 2007. Urban gridlock: macroscopic modeling and mitigation approaches. Transp. Res. Part B 41 (1), 49–62.
Daganzo, C.F., Geroliminis, N., 2008. An analytical approximation for the macroscopic fundamental diagram of urban traffic. Transp. Res. Part B 42, 771–781.
Daganzo, C.F., Gayah, V.V., Gonzales, E.J., 2011. Macroscopic relations of urban traffic variables: bifurcations, multivaluedness and instability. Transp. Res. Part B 45, 278–288.
Duives, D.C., Daamen, W., Hoogendoorn, S.P., 2015. Quantification of the level of crowdedness for pedestrian movements. Physica A 427, 162–180.
Geroliminis, N., Sun, J., 2011. Properties of a well-defined macroscopic fundamental diagram for urban traffic. Transp. Res. Part B 45 (3), 605–617.
Greenshields, D., 1947. The potential use of aerial photographs in traffic analysis. In: Highway Research Board Proceedings 27, HRB, National Research Council, Washington, D.C., pp. 291–297.
Haghani, M., Sarvi, M., 2016. Human exit choice in crowded built environments: investigating underlying behavioural differences between normal egress and emergency evacuations. Fire Saf. J. 85, 1–9.
Helbing, D., Molnar, P., 1995. Social force model for pedestrian dynamics. Phys. Rev. – Part E 51, 4282–4286.
Hoogendoorn, S.P., Bovy, P.H.L., 2002. Normative pedestrian behaviour theory and modelling. In: Taylor, M.A.P. (Ed.), Transportation and Traffic Theory in the 21st Century. Pergamon, Elsevier Science, Oxford, pp. 219–245.
Hoogendoorn, S., Bovy, P.H.L., 2003. Simulation of pedestrian flows by optimal control and differential games. Opt. Control Appl. Methods 24 (3), 153–172.
Hoogendoorn, S.P., Daamen, W., 2005. Pedestrian behavior at bottlenecks. Transp. Sci. 39 (2), 147–159.
Hoogendoorn, S.P., Campanella, M.C., Daamen, W., 2010. Macroscopic fundamental diagrams for pedestrian networks. Presented at 89th Annual Meeting of the Transportation Research Board, Washington, D.C.
Hoogendoorn, S.P., Campanella, M.C., Daamen, W., 2011. Fundamental diagrams for pedestrian networks. In: Peacock, R.D., Kuligowski, E.D., Averill, J.D. (Eds.), Pedestrian and Evacuation Dynamics 2011. Springer, New York, pp. 255–264.
Hoogendoorn, S.P., van Wageningen-Kessels, F., Daamen, W., Duives, D.C., Sarvi, M., 2015. Continuum theory for pedestrian traffic flow: local route choice modelling and its implications. Transp. Res. Part C: Emerg. Technol. 59, 183–197.
Johansson, A., 2009. Constant net-time headway as key mechanism behind pedestrian flow dynamics. Phys. Rev. E 80, 026120.
Knoop, V.L., van Lint, H., Hoogendoorn, S.P., 2015. Traffic dynamics: its impact on the macroscopic fundamental diagram. Physcia A: Stat. Mech. Appl. 438, 236–250.
Mazloumian, A., Geroliminis, N., Helbing, D., 2010. The spatial variability of vehicle densities as determinant of urban network capacity. Philosoph. Trans. Roy. Soc. A 368, 4627–4647.
Saberi, M., Mahmassani, H.S., 2014. Exploring areawide dynamics of pedestrian crowds: three-dimensional approach. Transp. Res. Rec.: J. Transp. Res. Board 2421, 31–40.
Underwood, R.T., 1961. Speed, volume and density relationships. Quality and Theory of Traffic Flow, Yale Bureau of Highway Traffic, pp. 141–188.
Weidmann, U., 1993. Transporttechnik der Fussgänger. Schriftenreihe des IVT 90. Institut für Verkehrsplanung.
Yang, X., Daamen, W., Hoogendoorn, S.P., Chen, Y., Dong, H., 2014. Breakdown phenomenon study in the bidirectional pedestrian flow. Transp. Res. Procedia 2, 456–461.
Zhang, J., Klingsch, W., Schadschneider, A., Seyfried, A., 2011. Transitions in pedestrian fundamental diagram of straight corridors and t-junctions. J. Stat. Mech: Theory Exp. 2011/6, P06004.
Zhang, J., Seyfried, A., 2013. Empirical characteristics of different types of pedestrian streams. Procedia Eng. 62, 655–662.